COBEM 99
XV Congresso Brasileiro de Engenharia Mecânica
15th Brazilian Congress of Mechanical Engineering
22 - 26 de Novembro de 1999 / November 22 - 26, 1999 Águas de Lindóia, São Paulo,

NUMERICAL ANALYSIS OF COAXIAL TURBULENT JETS IN DIFFUSERS AND CONTRACTIONS

Edimilson J. Braga
Marcelo J.S. de Lemos
Departamento de Energia - IEME
Instituto Tecnológico de Aeronáutica - ITA
12228-900 – São José dos Campos, SP, Brasil - E-mail: *mdelemos@tecsat.com.br*

Abstract. *Turbulent flow field calculations for confined coaxial streams are presented. The cases of turbulent flow in a gradually expanding/contracting conical duct, preceded and followed by a constant area section, are analyzed. Turbulence is modeled by means of the standard k-ε model since no strong curvature is of concern. A marching-forward numerical integration technique is used to sweep the computational domain. Within contractions, turbulence is damped, whereas in expansions the valued of k is increased. It was also found that turbulence kinetic energy levels are greater when the internal jet is faster than the annular stream.*

Keywords: *Turbulent jets, Coaxial Jets, Diffusers, Contractions. Turbulence Modeling*

1. INTRODUCTION

Turbulent jet flow through pipes with varying cross section represents an important class of engineering flows. Applications of such configurations are found in jet-pumps, rocket boosters, industrial piping and in air conditioning ducts.

Experimental work published on turbulent coaxial jets deals, in its majority, with sudden expansion flow into a stagnant surrounding (Buresti *et al*, 1998) or within a confining duct (Park & Chen, 1989). Measurements in two-phase systems (Albagli & Levy, 1991, Fan *et al*, 1996a) and computational studies applying Large Eddy Simulation to coaxial jets are also found in the literature (Knut & Moin, 1996). In all of the above, recirculating flow due to abrupt expansion precludes the use of the mathematical treatment below, which, in contrast, is based on a marching-forward technique (Patankar, 1988).

Yule & Damou, 1992, presented results for confined coaxial turbulent jets with velocity ratio U_1/U_2 up to 30, being U_1 the central jet velocity. Both streams flowed into a convergent - divergent channel. Report was limited to mean axial velocity and axial turbulent intensity. Yet, their overall duct length was of a relative short size (x/D = 4).

The compilation work of Spencer *et al*, 1995, seems to be the only available experimental data bank for turbulent flow within contractions and diffusers. Therein, experimental data from 11 institutions around the world, taken for flow of air and water in contraction and

diffuser, were compared with each other and with computational results using commercial CFD codes. The authors concluded that: “numerical simulation of turbulent flow through simple pipe components cannot be achieved with the commercial programs available”.

As a consequence of the above, the development of numerical tools for quick analysis of simple engineering flows, instead of using complex, memory demanding, large CFD codes, has motivated many research endeavors lately. If no recirculating motion is of concern (with mild streamline curvatures), marching-forward numerical techniques, implemented along with isotropic turbulence models, provide an economical means for engineering analysis with PC-based workstations.

Following this path, the work of Matsumoto and de Lemos, 1990, presented results for the developing *time-averaged* and *turbulent* fields in a coaxial jet along a circular duct of constant area. Later, de Lemos and Milan, 1997, extended their calculations to flow in long ducts with varying cross sections. Recently, de Lemos and Braga, 1998, simulated coaxial jets with *higher* ($U_e>U_i$) and *lower* ($U_e<U_i$) annular velocity in *diverging* ($H>0$) and *converging* ($H<0$) ducts with a *sinusoidal* wall. The present contribution applies the developed methodology to ducts with plane walls. A schematic is shown in figure 1. Also for this geometry the effects of damping of turbulence in contractions and its enhancement are diffusers is correctly calculated.

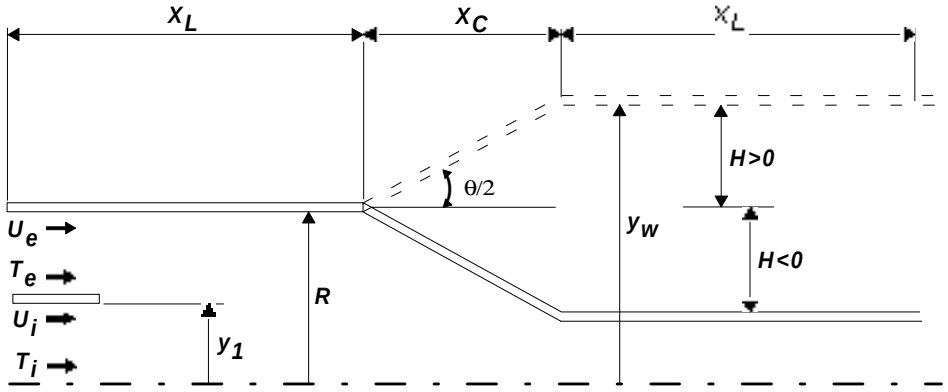

Figure 1 – Notation for general conical ducts with diverging and converging walls.

2. MATHEMATICAL MODEL AND NUMERICS

2.1 Mean flow

The equations of continuity of mass and axial momentum for a two-dimensional, source-free, low speed, planar/axi-symmetric turbulent mixing layer can be written as,

$$\frac{\partial\,(y^{\eta}\rho u)}{\partial x}+\frac{\partial\,(y^{\eta}\rho v)}{\partial y}=0 \tag{1}$$

$$\rho u\frac{\partial u}{\partial x}+\rho v\frac{\partial u}{\partial y}=-\frac{\partial P}{\partial x}+\frac{1}{y^{\eta}}\frac{\partial}{\partial y}\left[y^{\eta}\ \mu_{eff}\frac{\partial u}{\partial y}\right] \tag{2}$$

In Eq. (1) and Eq. (2) u, v are the velocity components in the axial and transverse direction, respectively, ρ the fluid density, P the static pressure, and μ_{eff} the coefficient of

turbulent exchange given as $\mu_{eff} = \mu_t + \mu$. Also, μ and μ_t are the molecular and turbulent viscosity, respectively. As usual, equations (1) and (2) are written in a compact notation embracing planar (η=0) and axi-symmetric (η=1) cases.

2.2 Turbulence model

The statistical turbulence model k-ε (Jones and Launder, 1972) has been extensively used in the literature for its characteristics of robustness and numerical stability. The diffusion-like character of turbulent transport is mostly responsible for improved stability of the model. Recent extensions of its applicability to a wide variety of flows include the so-called **RNG** and **Non-Linear** approaches. Basically, the model embodies the early idea of Prandtl/Kolmogorov that, in a turbulent flow, the apparent viscosity μ_t can be considered as proportional to the product of a characteristic velocity scale V' and a characteristic length scale L'. In the k-ε model, the characteristic velocity scale is given by $V'=k^{1/2}$, and the characteristic length scale is written as $L'=k^{3/2}/\varepsilon$. Both scales imply for the turbulent viscosity $\mu_t = \rho\, c_\mu\, k^2/\varepsilon$, where c_μ is a constant. Here, only the case involving flow regions of high local Reynolds numbers, or say, regions with Kolmogorov and macroscopic scales adequately separated, is considered (Launder and Spalding, 1974). With this, transport equations for k and ε can be written as,

$$\begin{aligned} \rho u \frac{\partial k}{\partial x} + \rho v \frac{\partial k}{\partial y} &= \frac{1}{y^\eta}\frac{\partial}{\partial y}\left[y^\eta\ \Gamma_k \frac{\partial k}{\partial y}\right] + S_k \\ \rho u \frac{\partial \varepsilon}{\partial x} + \rho v \frac{\partial \varepsilon}{\partial y} &= \frac{1}{y^\eta}\frac{\partial}{\partial y}\left[y^\eta\ \Gamma_\varepsilon \frac{\partial \varepsilon}{\partial y}\right] + S_\varepsilon \end{aligned} \qquad (3)$$

In Eq. (3) Γ_k and Γ_ε are given by $\Gamma_k = \mu + \mu_t/\sigma_k$; $\Gamma_\varepsilon = \mu + \mu_t/\sigma_\varepsilon$ where the σ's are the turbulent Prandtl/Schmidt numbers for k and ε, respectively. The last terms in Eq. (3) are known as "source" terms and are given by $S_k = \rho\,(P_k - \varepsilon)$ and $S_\varepsilon = \rho\,\varepsilon/k\,(c_1 P_k - c_2 \varepsilon)$. The constants take their usual values, namely c_1=1.47, c_2=1.92 and c_μ=0.09. Further, the production term reads $P_k = \mu_t/\rho\ (\partial U/\partial y)^2$.

2.3 Boundary conditions and computational details

The numerical approach here adopted is the well-known parabolic solver technique of Patankar and Spalding, 1972, and Patankar, 1980. Inlet flow for the central and annular jets are given a uniform distribution defining the velocity ratio U_i/U_e, where U_i and U_e are the inlet velocities for the central and annular regions, respectively. The inlet values for k and ε were assumed as $k_{in} = 10^{-3} U_m^2$ and $\varepsilon_{in} = k_{in}^{3/2}/\mathrm{K}y'$ where U_m is the overall mean velocity, K is the von Kármán constant (K=0.4) and y' is the distance to the wall. Also, for the centerline (y=0), the symmetry condition was implemented for all dependent variables as $\partial\phi/\partial y\big)_{y=0} = 0$ where $\phi = U$, k and ε.

2.4 Wall treatment

Wall proximity is handled by the usual **Wall Function** approach (Launder and Spalding, 1972, Launder and Spalding, 1974), giving for the wall shear stress,

$$\tau_w = \left(U_N \rho c_\mu^{1/4} k_N^{1/2}\right) \Big/ \frac{1}{\mathrm{K}} \ln\left[E\, y_N \frac{\rho (c_\mu^{1/2} k_N)^{1/2}}{\mu}\right] \tag{4}$$

where E is a constant. In Eq. (4) the subscript "N" identifies the grid point closest to the wall. In that region, the use of the Wall Function associated with the assumption of "local equilibrium" for turbulence (P_k=ε) gives $k_N = \tau_w / (\rho c_\mu)^{1/2}$; $\varepsilon_N = k_N^{3/2} / \mathrm{K}\, y_N$. Rewriting Eq. (4) in the form $\tau_w = \lambda \mu (\partial U / \partial y)$ gives further,

$$\lambda = \begin{cases} 1 \quad \text{for laminar flow} \\ \dfrac{\mathrm{K}\, y_N \dfrac{\rho (c_\mu^{1/2} k_N)^{1/2}}{\mu}}{\ln\left[E\, y_N \dfrac{\rho (c_\mu^{1/2} k_N)^{1/2}}{\mu}\right]} \quad \text{for turbulent flow} \end{cases} \tag{6}$$

2.5 Pressure gradient

Determination of the unknown pressure gradient is handled exactly as explained in Patankar, 1988. That approach consists basically in finding the "zero" of a function *f(dP/dx)* defined as;

$$f(dp/dx) = \left(A_{calc} - A_{duct}\right) / \Psi_{EI} \tag{7}$$

Table 1 – Input data for geometry of Figure 1

	Long duct - U_i/U_e=1		Short duct, y_1/D=0.5			
			U_i/U_e=1.30		U_i/U_e=0.76	
	Div.	Con.	Div.	Con.	Div.	Con.
Limits for H/D	+.3	-.3	.3	-.3	.3	-.3
X_L/D	100		5			
X_c/D	25					

where the left hand side represents the discrepancy, at the downstream position, between the *calculated* and *real* duct areas. Solution of Eq. (7) can be achieved with an iterative Newton-Raphson method of the form;

$$f^* + f^{*'}\left[(dp/dx) - (dp/dx)^*\right] = 0 \tag{8}$$

where "starred" values are estimated quantities later improved in subsequent iterations. Typically, 3 to 4 iterations are necessary in solving Eq. (8) at each axial station. It is worth noting that applicability of the model above is limited to parabolic flow analyses, so that recirculating motion induced by boundary layer separation in fast diverging ducts or *"vena contracta"* regions after duct constrictions are not considered here. With these restrictions applied, the axial momentum equation can be solved with well-known marching-forward numerical techniques for computation of parabolic and partially parabolic flows.

3. RESULTS AND DISCUSSION

The flow field in the duct shown in Fig. 1 was calculated with two sets of input data. The first one consisted of a long inlet region followed by a converging/diverging duct before another long outlet sector was calculated. In this case, at entrance, the concentric jets were of equal value, or say U_i/U_e=1. The objective of this case was to investigate the changes in fully developed profiles occurring past an area changing section without the simultaneous hydrodynamic boundary-layer development at the wall. Then, changes in the mean and turbulent quantities, solely due to duct area variation, could be isolated for analysis. The second case involves the use of a short tube length before and after a conical wall section.

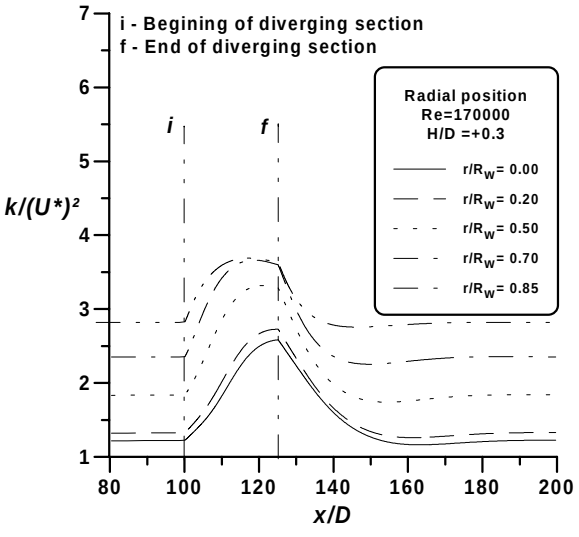

Figure 2- Axial behaviour of k/U^{*2} for several radial positions along an expansion.

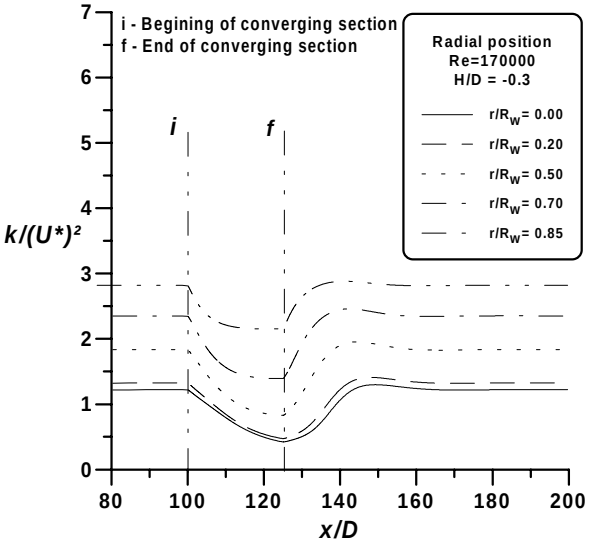

Figure 3– Axial behavior of k/U^{*2} for several radial positions along a contraction.

This short duct case had a small entrance length of X_L/D = 5 with jet velocity ratios U_i/U_e equal to 0.76 and 1.30. This situation was concerned with mixing of streams at different velocities, embracing velocity rations higher and lower than unity. The former case was aimed at the analysis of fully developed flow passing by an obstruction or expansion whereas the

latter situation was used to simulate the mixing of streams past ducts with varying cross section. Either expansion or contraction of the initial duct area was based on a variation up to 30% of the initial duct radius. Data used in all cases are summarized in Table 1.

3.1 Long duct

Calculations for long ducts were discussed in de Lemos and Milan, 1997, and a few results are here included for clarity. The behavior of turbulence along an area changing section is shown in Fig. 2 and Fig 3. The figures present the non-dimensional turbulent kinetic energy along the duct and at different radial positions. It is interesting to note that in the diverging duct, Fig. 2 indicates that within the flow domain an increase in k/U^{*2} takes place across the entire cross section. An opposite trend is shown in Fig. 3. Yet, this change in the fully developed profiles reaches a maximum value before and around the end of the diverging/converging section (x/D=125), requiring nearly another 25 to 30 diameters downstream the flow in order to smooth out the observed streamwise spatial variations. The results herein confirm also similar computations presented in de Lemos and Braga, 1998, for ducts with sinusoidal walls. If the centerline behavior for k/U^{*2} is plotted for $-0.3<H/D<0.3$ as in Fig. 4, one can further note the effect of enlargement/contraction on enhancement/damping of turbulence.

3.2 Short duct

Calculations were then performed in a 25 diameters long diverging/converging section preceded and followed by a length equal to x/D=5. In the first case, an internal jet with velocity 30% higher than the concentric external stream ($U_i>U_e$) was considered. For comparison, the case of a higher velocity external stream was also computed (U_e/U_i=1.3).

Mean velocity profiles are presented in Fig. 5 and Fig. 6 for U_i/U_e=1.3. Relative deceleration of the central flow (reduction of u/U_m) in Fig. 6 is much stronger than in Fig. 5. Stronger flattening of the velocity profile in converging ducts may suggest the use of this geometry for quickly mixing coaxial jets with higher inner velocity.

The behavior of corresponding turbulent fields is shown in Fig. 7 and Fig. 8. The steep velocity gradient at the duct entrance promotes turbulence production increasing the level of k within the mixing layer. Later downstream, this energy level is dissipated by diffusion to the center and wall regions. In Fig. 7, most k values lie above those at the initial position x/D=5.

On the other hand, in Fig. 8, calculated k profiles are equal or lower than the initial position values (at x/D=5). Therefore, enhanced turbulence energy within diverging ducts as well as damped turbulence in a contraction are clearly seen in the figures.

Similar results are presented when the external jet velocity is higher than the internal one. Fig. 9 and Fig. 10 show mean velocity profiles whereas Fig. 11 and Fig. 12 present turbulent parameters. The double humped profiles in Fig. 9 and Fig.10, not presented in Fig. 5 and Fig. 6, evolve to a bulged form in expansions and to a flatter distribution in contractions. In Fig. 9 and Fig. 10 mean velocity gradients, in most of the duct, are lower than those when U_i is higher than U_e. This is seen by comparing corresponding Figs. 5-6 with Figs. 9-10.

Consequently, overall k levels, when $U_e>U_i$, are expected to be lower than those of Fig. 7 and Fig. 8. Accordingly, this is confirmed when inspecting both sets of Figs. 7-8 and Figs. 11-12. Also seen, when comparing Figs. 8 and 12, is that damping of turbulence is more effective when U_e is greater than U_i. In a similar manner, enhancement of k in Fig. 7 is more pronounced than in Fig. 11, showing that jet flows with $U_i>U_e$ are preferable when mixtures with high turbulent intensities are sought. Additional comments on the influence of U profiles on the overall value of k are presented below.

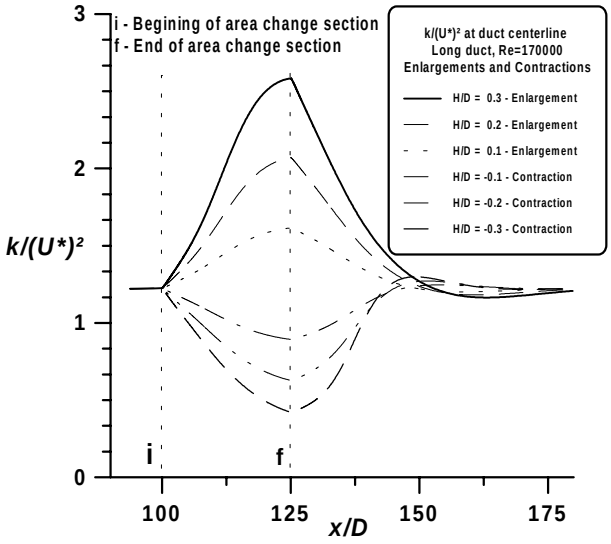

Figure 4 – Turbulent kinetic energy along centerline for enlargements and contraction.

Figure 11 and Fig. 14 compare the centerline development of k/U^{*2} for the mixing of streams in different channels and with different inlet velocity ratios. Fig. 11 ($U_i>U_e$) indicates that in this radial position, a reduction on the level of the turbulent kinetic energy in the converging duct occurs due to the relative retardation of the core velocity causing a flatter U profile at the center and, consequently, a lower level of k. The mean field acquires more kinetic energy but a lower fraction is made available for generating turbulence.

On the other hand, in the expanding duct, retardation of wall fluid layers increases k production rate at the center and, although the mean flow kinetic energy is reduced - by transformation of kinetic on pressure energy during duct enlargement - a higher percentage is turned into turbulence by the action of the steep gradients occurring within the flow.

Figure 14, for $U_e>U_i$, also presents higher values at the centerline for k in diverging geometries. However, in this figure, the overall turbulence level is lower than those presented in Fig. 11. By comparing Fig. 5 and Fig. 9 one can see that within the region $0.3<y/R<0.6$, gradients in the double humped u/U_m profile Fig. 9, responsible for k production, undergo a change in sign. On the other hand, in Fig. 5, the higher velocity in the bulk of the flow tend to keep reasonable gradients of mean velocity along all duct. Levels of k are then higher when the internal jet is faster than the external stream. Later, at the duct exit and after most mixing has occurred (x/D=35), both cases present similar values for k, independent of the incoming jet configuration.

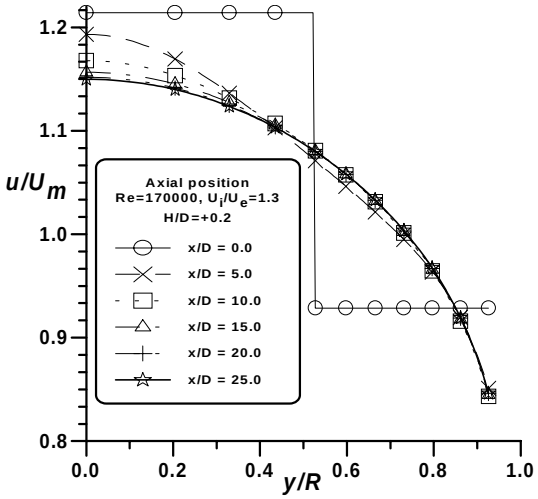

Figure 5 – Mixing streams along expansion.

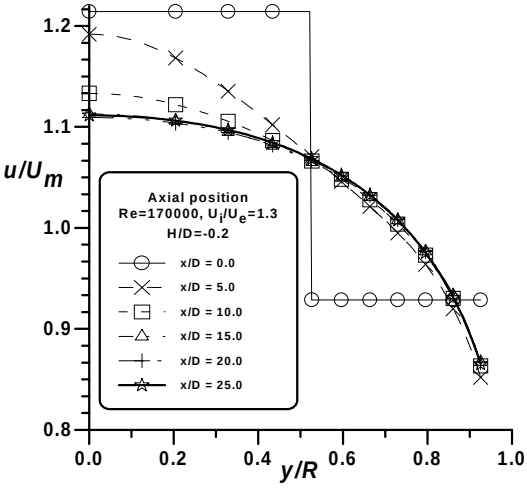

Figure 6 – Mixing streams along contraction.

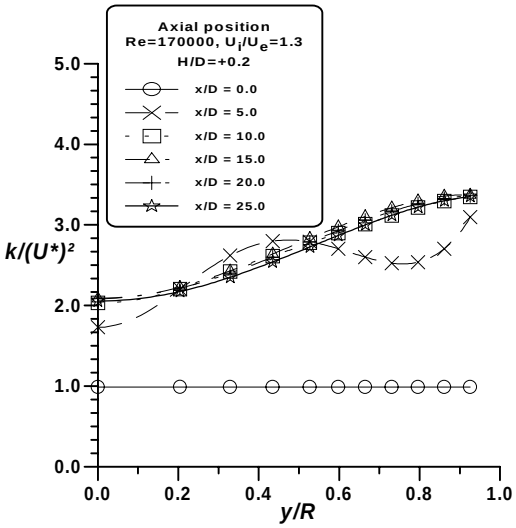

Figure 7 – Profiles of turbulent kinetic energy along expansion.

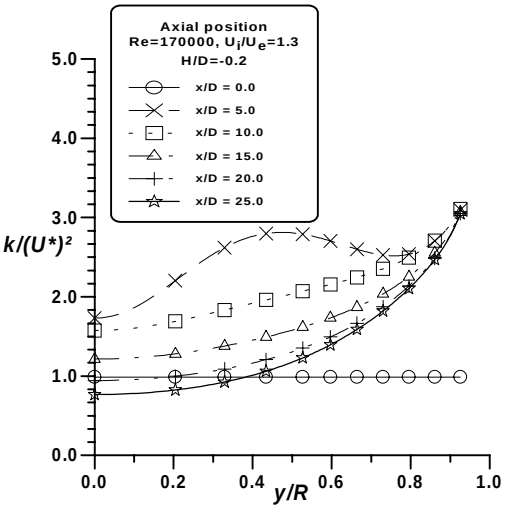

Figure 8 – Turbulent kinetic energy along contraction.

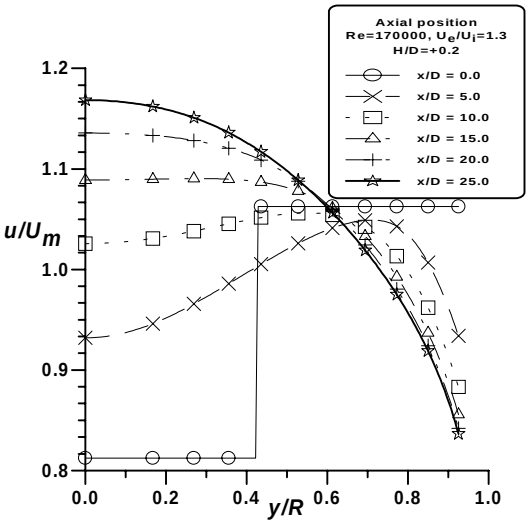

Figure 9 – Mixing streams along expansion.

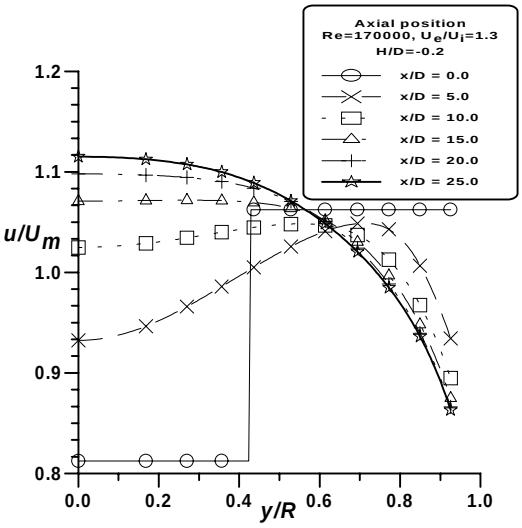

Figure 10 – Mixing stream along contraction.

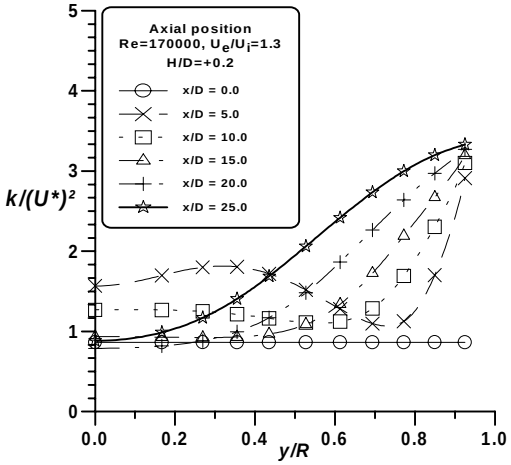

Figure 11 – Mixing stream along expansion.

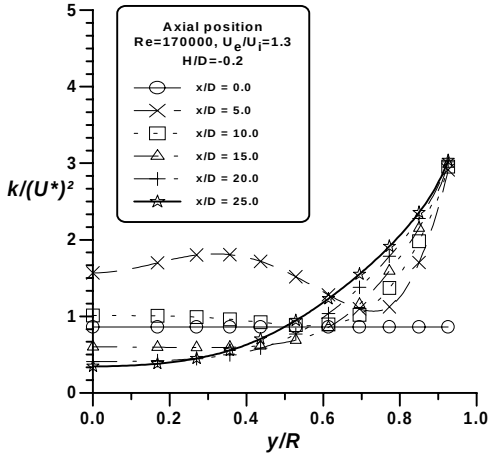

Figure 12 – Turbulent kinetic energy along contraction

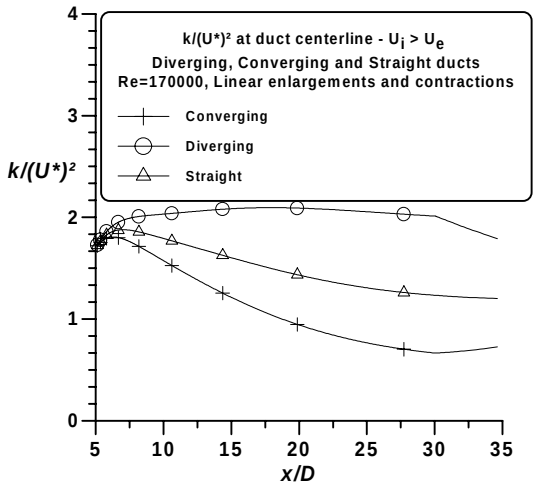

Figure 13 – Centerline turbulent kinetic energy development.

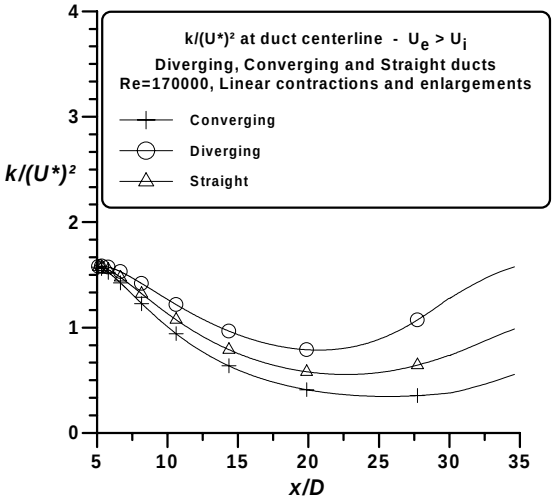

Figure 14 – Centerline turbulent kinetic energy.

4. CONCLUDING REMARKS

This paper presented computations with the k-ε model for simulation of confined jet flow in ducts of varying cross-section. Diverging and converging plane ducts were calculated showing different behavior for the mean and turbulent fields. In general, accelerated flows in a convergent duct reduce turbulence level, eventually leading to laminarization of the flow (Jones and Launder, 1972). Flattening of the velocity profile in converging ducts may suggest the use of this geometry for rapidly mixing coaxial jets with a higher internal velocity. Based on the foregoing, it is expected that the results herein can contribute to the design and analysis of engineering equipment involving concentric turbulent ducts. Potential application may also include fluid machinery development.

Acknowledgements

The authors are thankful to CNPq, Brazil, for their financial support during the course of this research.

REFERENCES

Albagli, D., Levy, Y., 1991, EXPERIMENTAL STUDY ON CONFINED TWO-PHASE JETS, *Journal of Thermophysics and Heat Transfer*, v. 5. n. 3, pp. 387-393.

Buresti, G., Petagna, P., Talamelli, A., 1998,EXPERIMENTAL INVESTIGATION ON THE TURBULENT NEAR-FIELD OF COAXIAL JETS, *Experimental Thermal and Fluid Science*, v 17, n. 1-2, pp. 18-26.

de Lemos, M.J.S., Braga, E.J., 1998, NUMERICAL INVESTIGATION OF TURBULENT DUCT FLOW THROUGH GRADUAL ENLARGEMENTS AND CONTRACTIONS, ASME-FED-vol. 245, Paper FEDSM98-4886, ISBN: 0-7918-1950-7.

de Lemos, M.J.S., Milan, A., 1997, MIXING OF CONFINED COAXIAL TURBULENT JETS IN DUCTS OF VARYING CROSS SECTION, *CD-ROM of COBEM97 – 12th. Braz. Cong. Mech Eng*., Bauru, São Paulo, Brazil, December 8-12.

Fan, J.; Zhao, H., Cen, K., 1996a, TWO-PHASE VELOCITY MEASUREMENTS IN PARTICLE-LADEN COAXIAL JETS, *Chemical Engineering Journal*, v. 63, n. 1, p. 11-17.

Jones, W.P., Launder, B.E., 1972, THE PREDICTION OF LAMINARIZATION WITH A TWO-EQUATION MODEL OF TURBULENCE, Int. J. Heat & Mass Transfer, vol. 15, pp. 301-314.

Knut, A, Moin, P., 1996, LARGE-EDDY SIMULATION OF TURBULENT CONFINED COANNULAR JETS, *Journal of Fluid Mechanics,* vol. 315, p. 387-411.

Launder, B.E., Spalding, D.B. 1972, LECTURES IN MATHEMATICAL MODELS OF TURBULENCE, Academic Press, New York.

Launder, B.E., Spalding, D.B., 1974, THE NUMERICAL COMPUTATION OF TURBULENT FLOWS, Comp. Meth. App. Mech. Eng., vol. 3, pp. 269-289.

Matsumoto, E. & de Lemos, M.J.S., 1990, M.J.S., DEVELOPMENT OF AN AXI-SYMMETRIC MIXING LAYER IN A DUCT OF CONSTANT CROSS SECTION, *Proc. of 3rd Braz. Therm. Sci. Meet.*, vol. I, pp. 381-385, Itapema, Brazil, December 10-12.

Park, C.J.; Chen, L.D., 1989, EXPERIMENTAL INVESTIGATION OF CONFINED TURBULENT JETS. PART I. SINGLE-PHASE DATA, *AIAA Journal*, v. 27, n. 11, pp. 1506-1510.

Patankar, S.V., 1980, NUMERICAL HEAT TRANSFER AND FLUID FLOW, Mc-Graw Hill.

Patankar, S.V., 1988, PARABOLIC SYSTEMS, Chapter 2 of HANDBOOK OF NUMERICAL HEAT TRANSFER, Rohsenow ed., John Wiley & Sons, New York.

Patankar, S.V., Spalding, D.B., 1972, A CALCULATION PROCEDURE FOR HEAT, MASS AND MOMENTUM TRANSFER IN THREE-DIMENSIONAL PARABOLIC FLOWS, *Int. J. Heat & Mass Transf.*, vol. 15, pp. 1787-1806.

Spencer, E.A., Heitor, M.V., Castro, I.P., 1995, INTERCOMPARISON OF MEASUREMENTS AND COMPUTATIONS OF FLOW THROUGH A CONTRACTION AND A DIFFUSER, *Flow Measurement and Instrumentation,* v. 6, n. 1, p. 3-14.

Yule, A.J., Damou, M., 1992, AXISYMMETRICAL TURBULENT JET FLOWS IN A DUCT OF VARYING AREA, *Experim. Thermal and Fluid Science*, v. 5, n. 4, p. 499-505.